



## Evolution of self-generating porous microstructures in polyacrylonitrile-cellulose acetate blend fibres

Suntharavathanan Mahalingam <sup>a</sup>, Xiaowen Wu <sup>b</sup>, Mohan Edirisinghe <sup>a,\*</sup>

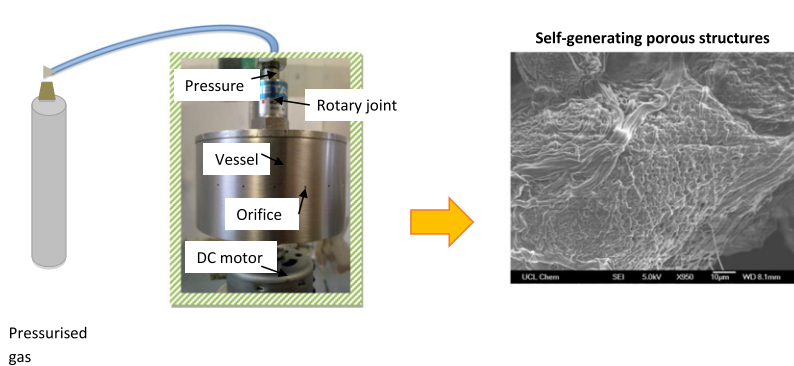
<sup>a</sup> Department of Mechanical Engineering, University College London, Torrington Place, London WC1E 7JE, UK

<sup>b</sup> School of Materials Science and Technology, China University of Geosciences, 29 Xueyuan Road, Beijing 100083, China

### HIGHLIGHTS

- Gyration under pressure was used to spin polyacrylonitrile-cellulose acetate blend fibres.
- Self-generating porous structures were obtained by controlling working pressure.
- Artificial porous fibrous structures were made by leaching and etching.
- Structural evolution in polyacrylonitrile-cellulose acetate blend fibres is explained.
- A mathematical model has been developed to predict fibre diameter.

### GRAPHICAL ABSTRACT



### ARTICLE INFO

#### Article history:

Received 22 May 2017

Received in revised form 17 July 2017

Accepted 24 July 2017

Available online 3 August 2017

#### Keywords:

Polymer  
Fibre  
Composite  
Porous  
Self-generating  
Pressure  
Gyration

### ABSTRACT

Polyacrylonitrile (PAN), cellulose acetate (CA) and polyacrylonitrile - cellulose acetate (PAN-CA) fibres were formed in single and binary solvents which were subjected to gyration under pressure. Fibres in the diameter range 200–2000 nm were generated using a rotating speed of 36,000 rpm and a working pressure of  $3 \times 10^5$  Pa. Long fibre morphologies with isotropic distribution of fibre orientation were obtained from PAN polymer solutions with a concentration of 5–15 wt%. Short fibre morphologies with anisotropic distribution of fibre orientation were produced for CA polymer solutions with a concentration of 25 wt% and below this concentration polygonal beads were generated. PAN-CA fibre bundles were generated and these showed remarkable self-generating porous characteristics when the working pressure was changed from 1 to  $3 \times 10^5$  Pa. For comparison, porous PAN-CA fibres were also generated by solvent etching and porogen leaching techniques and in these the etching time and porogen concentration influenced the pore size of the generated fibres. Fourier transform infrared and Raman spectroscopies were performed to elucidate the bonding characteristics in the fibres. Release characteristics of the porous fibrous structures were studied using vanillin as the active ingredient. A mathematical model which allows the evaluation of the fibre diameter as a function of rotating speed and working pressure is presented and this helps to understand the solvent mass transfer taking place during fibre forming.

© 2017 The Author(s). Published by Elsevier Ltd. This is an open access article under the CC BY license (<http://creativecommons.org/licenses/by/4.0/>).

### 1. Introduction

Porous fibres are excellent candidates for enhanced photocatalytic activities owing to their high surface area, attendant dispersions of catalyst functions and superior mass transport. It has been shown that

\* Corresponding author.

E-mail address: [m.edirisinghe@ucl.ac.uk](mailto:m.edirisinghe@ucl.ac.uk) (M. Edirisinghe).

TiO<sub>2</sub>/SiO<sub>2</sub> porous fibres had significantly enhanced photocatalytic activity and photodegradation of rhodamine compared to TiO<sub>2</sub> nanoparticles and Degussa P25 [1]. Highly porous graphitic fibres are widely used as a counter electrode in dye sensitised solar cells with high photoconversion performance. Using porous fibres is an ideal strategy for improving the surface of electrodes which in turn influences the rate of electrochemical reaction [2]. These designed architectures have been also exploited in lithium ion batteries and supercapacitors which offer improved energy and power density [3,4]. The potential use of porous polycaprolactone fibres in tissue engineering scaffolds has been reported by evaluating mouse osteoblast cell growth in them and results show excellent cell attachment and proliferation [5,6].

A plethora of methods have been used to generate porous fibres and increase their porosity. Of these, the phase separation method is widely reported, where selected removal of one polymer after spinning a polymer blend from solutions is used to generate multi-phase fibres [7]. Here, when the polymer blend solution becomes thermodynamically unstable and if one of the dispersed phases can be accessed and removed easily without collapse, then internal pores could be created in the fibres [8]. Another method involves using porogens during fibre forming and subsequent leaching out the porogens is done post-processing. For example, removing CaCO<sub>3</sub> in PAN/CaCO<sub>3</sub> fibres using an extraction bath containing HCl/water at various temperature and time intervals can generate porous structures [9]. Alternatively, pores could be formed using a humid environment, in this case water molecules from the atmosphere condense on the surface to leave imprints on fibres [10,11]. However, these methods are not robust and lack simplicity, most of them require post-processing which is time consuming and costly. In addition, the residual additives used in such operations could affect the quality of formed fibres.

Polyacrylonitrile (PAN) is a well-known precursor for carbon fibres, it has a high carbon yield as well as outstanding mechanical properties [12,13]. PAN is a semi-crystalline synthetic polymer obtained through free radical polymerisation of acrylonitrile. The non-meltable ladder structure obtained through cyclisation of PAN molecules is very crucial to avoid melting during carbonisation. The cyclised network of hexagonal carbon nitrogen rings are formed with nitrile groups through a thermal free radical mechanism [14]. Nitrile groups in PAN also have a large dipole moments and provide high cohesive energy density and chain stiffness which result in excellent tensile strength. Cellulose acetate (CA) is a semi-synthetic polymer derived from cellulose which is the most common biopolymer used in biomedical applications such as tissue engineering and drug delivery [15–17]. Cellulose acetate is derived from esterification of cellulose, which is obtained by reaction of cellulose with acetic anhydride and acetic acid in the presence of sulphuric acid.

Pressurised gyration is an attractive method concurrently using centrifugal spinning and solution blowing to form large quantities of nanofibres [18]. The process depends on the concentration of the solute-solvent mixture, rotating speed of the gyration vessel and the working pressure across an orifice to generate fibres on a scale range from nano- to micro-. Thus, this method offers not only control of the polymeric nanofibre diameter and length but also their size distribution [18]. A mathematical model illustrating how the fibres are generated in this process has been described by considering rotational and blowing frames of the spinning process [19]. It is an uncomplicated but efficient technique permitting simultaneous generation of a multitude of polymer nanofibres with regular morphology [20–22]. In addition, pressurised gyration has shown to generate functional microbubbles (rather than fibre) that could be used in drug delivery, antimicrobial vesicles and biosensing [23,24].

The current work discovers a new route to form well characterised self-generating porous polyacrylonitrile-cellulose acetate composite fibres using pressurised gyration. This forming process relies on the destabilising centrifugal force and the dynamic fluid flow acting against the stabilising surface tension of the polymer solution to form fibres at

very high speed. By carefully tuning one of the process parameters, working pressure, porous composite fibres were obtained. Here we use the well-known synthetic polymer polyacrylonitrile in combination with a semi-synthetic polymer derived from natural cellulose to form porous structures. Moreover, for comparison, in this study porous fibres are also made from post-processing techniques such as porogen leaching (sodium chloride) and solvent etching. We describe in detail plausible explanations for forming porous fibrous structures using these routes. Taking vanillin as a model material, the release characteristics of active ingredients from these structures in de-ionised water is studied and findings discussed. We give details of the mechanism of sorption of such active ingredient molecules and their release profile from the porous fibrous structures.

## 2. Materials and methods

### 2.1. Materials

Polyacrylonitrile (PAN) ( $M_w = 150$  kDa) and cellulose acetate (CA) ( $M_w = 30$  kDa) were used as received from Sigma Aldrich, UK. Acetone and dimethylformamide (DMF) were obtained from Sigma Aldrich, UK. Vanillin (Kosher) was purchased from Sigma Aldrich, UK and used as received.

### 2.2. Solution preparation and characterisation

Various concentrations of PAN solutions (5, 10, 15 wt%) were prepared by dissolving PAN powder in DMF and mixing using a magnetic stirrer for 24 h at ambient temperature (~20 °C). Similarly, various concentrations of CA solutions (15, 20, 25 wt%) were prepared by dissolving CA in acetone/DMF solvent mixture. These solutions were subjected to rigorous mixing by a magnetic stirrer until CA was completely dissolved. In addition, 10 wt% PAN-CA composite polymer solution was prepared in acetone/DMF solvent mixture. Various ratios of solvent mixture were used for this study. Of these the 2:1 ratio was chosen as an optimum mixture for this work.

The prepared polymer solutions were characterised by measuring their physical properties such as viscosity and surface tension (Table 1). A Kruss tensiometer K9 was selected and used for measuring the surface tension of the solutions (Wilhelmy plate method). A Brookfield viscometer was used to measure the viscosity of the polymer solutions. All equipment was calibrated before use and all measurements were performed at ambient conditions (20 °C and 42% relative humidity).

### 2.3. Fibre preparation

Fibres of PAN, CA and PAN-CA were prepared using pressurised gyration. The experimental set up used at the ambient temperature in this study is schematically illustrated in Fig. 1. It consists of a rotary aluminium cylinder vessel with ~60 mm diameter and ~35 mm height. There are approximately 20 orifices located on the wall of vessel, and each is ~0.5 mm in diameter. The features of orifices (number, dimensions and shape) and vessel could be customized. The vessel is driven by a DC motor which connects at the bottom of vessel, and it could

**Table 1**

Polymer solutions' physical properties obtained at ~20 °C.

Polymer solution	Surface tension (mN/m)	Viscosity (mPa s)
5 wt% PAN	52.5	200
10 wt% PAN	56.0	760
15 wt% PAN	58.0	1090
15 wt% CA	57.0	75
20 wt% CA	59.0	230
25 wt% CA	61.0	650
10 wt% PAN-CA	53.0	740

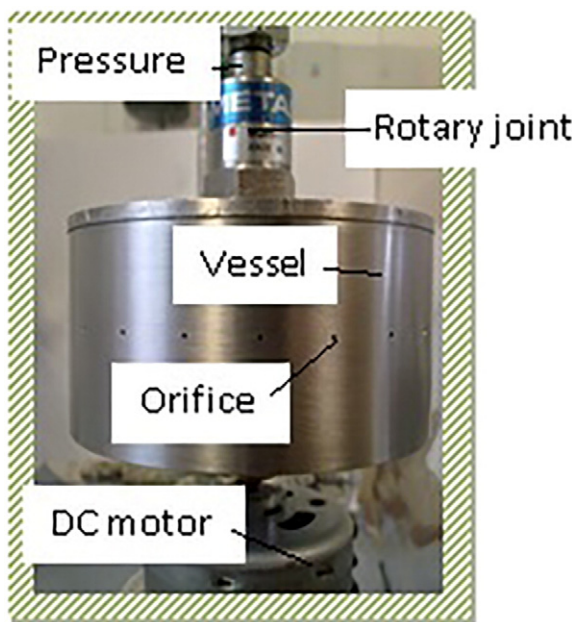


**Fig. 1.** Pressurised gyration equipment used in this research to form self-generating porous fibres.

work in the range 4.5 to 15 V in order to provide various rotating speeds up to 36,000 rpm. The applied pressure (up to  $3 \times 10^5$  Pa) was provided by a nitrogen cylinder connected to the top of the vessel. A stationary aluminium foil served as the collector and was placed around the vessel which helps convenient fibre collection. The collection distance used in this work was 70 mm. The process is illustrated in a video given as Supplementary Information at <http://www.materialsviews.com/growing-polymer-nanofibres-with-ease/>.

Self-generating porous fibres of PAN-CA composites were made by tuning the working pressure appropriately at constant rotating speed. Porous structures were also deliberately made by post-processing the fibres made by gyration without any working pressure. Of these, in solvent etching, the composite fibres made were etched in acetone/DMF solution at various time intervals between 5 and 30 min to change the pore size. **Table 2** shows the etching times and the corresponding pore sizes obtained in this investigation. In the leaching process, different concentrations of NaCl crystals were incorporated in the initial polymer composite solution and then they were leached out in de-ionised water to form the pores in the fibres. **Table 3** shows the concentration of NaCl and the corresponding pore sizes in this investigation.

#### 2.4. Structural characterisation

Fibre morphology was investigated with a JSM-6301F scanning electron microscope (SEM). Before imaging, all samples were coated with gold using a Quorum Q 150R ES sputter machine for 120 s in order to minimize charging effects. The micrographs were recorded at an operating voltage between 5 and 20 kV and an emission current 6  $\mu\text{A}$  to get

**Table 2**

Relationship between etching time and pore size of the fibres, obtained after post processing.

Etching time in DMF/acetone (minute)	Pore size ( $\mu\text{m}$ )
5	$0.67 \pm 0.50$
10	$2.44 \pm 1.00$
15	$5.06 \pm 2.70$
20	$6.54 \pm 2.24$
25	$8.94 \pm 1.61$
30	$9.42 \pm 3.27$

**Table 3**

Relationship between NaCl concentration and pore size of the fibres, obtained after post processing.

NaCl concentration (wt%)	Pore size ( $\mu\text{m}$ )
0.2	$1.37 \pm 0.55$
0.4	$2.51 \pm 1.35$
0.6	$2.70 \pm 0.97$
0.8	$3.44 \pm 1.42$
1.0	$4.06 \pm 1.79$

high resolution pictures. The images obtained were used to analyse the fibre and pore size.

Thermogravimetric analysis (TGA) was carried using PAN-CA blended fibres in a computer controlled Netzsch Thermobalance. The tests were carried in a nitrogen environment. A sample mass of 3.3 mg was heated at 5 °C/min from 27 °C to 400 °C.

Brunauer-Emmett-Teller (BET) analysis of the surface area of the PAN-CA fibres were determined using an automated surface area and pore size analyser (Quantachrome, Quadrasorb EVO). The fibres were degassed at 80 °C under vacuum for 18 h to remove any contaminating molecules from fibrous surface. For the determination of surface area the relative pressure ( $P/P_0$ ) in the range 0.01–0.25 was used, and nitrogen was used as the adsorbing gas. The specific surface area was calculated using the multipoint BET method and the pore size distribution was determined from the nitrogen adsorption isotherms using the density function theory (DFT).

FTIR spectrometer (Bruker-Alpha) equipped with an attenuated total reflectance (ATR) probe attachment along with an internal reflectance element (IRE) germanium (Ge) crystal at an end-face angle of 45° was used to obtain Fourier transform infrared (FTIR) spectra which was recorded in the wavelength range 400–4000  $\text{cm}^{-1}$ . The data was used to evaluate the interfacial interaction between polymer blend constituents in the composite fibres.

Raman microscope (inVia™ Renishaw) excited with 633 nm incident wavelength radiation was used to acquire Raman measurements on the samples. The data acquisition covered the spectral range 3000–100  $\text{cm}^{-1}$  with a spatial resolution of 4  $\text{cm}^{-1}$ . Raman data was baseline corrected.

Ultraviolet-visible spectroscopy studies (UV-Vis spectroscopy) were performed on the samples to study the release characteristics of vanillin in de-ionised water. UV-Vis absorption spectra were obtained using a Perkin Elmer Lambda 35 spectrometer with a 4 nm spectral resolution at 25 °C in the 200–700 nm wavelength range. Initially porous fibres were coated with vanillin by dipping in 10 wt% vanillin solution for 24 h and then they were immersed in de-ionised water at various temperatures to evaluate the release profile. The number of adsorbed vanillin molecules in the porous fibres were calculated to be  $41 \times 10^{20}$ .

The residual NaCl particles in the gyrospun leached fibres were evaluated using the following procedure. Initially, the fibres were washed in de-ionised water several times and dried. This was to ensure the complete dissolution of NaCl residues in the fibres. Thereafter, the fibres were dissolved in solvent acetone/DMF mixture to extract the NaCl residues that were trapped inside the fibres. The concentration of the chloride ions were measured by precision chlorine test paper. The dry test paper strip was dipped into solution to be tested, without any agitation and compared immediately with the colour chart provided by the supplier (Precision Laboratories, USA).

## 3. Results and discussion

### 3.1. Effect of polymer solutions' physical properties on formability of fibres

The initial setting up of process control parameters for forming fibres by pressurised gyration are crucially governed by the characteristics of polymer solutions' physical properties. Thus, the quality of the products generated in pressurised gyration depend on surface tension and

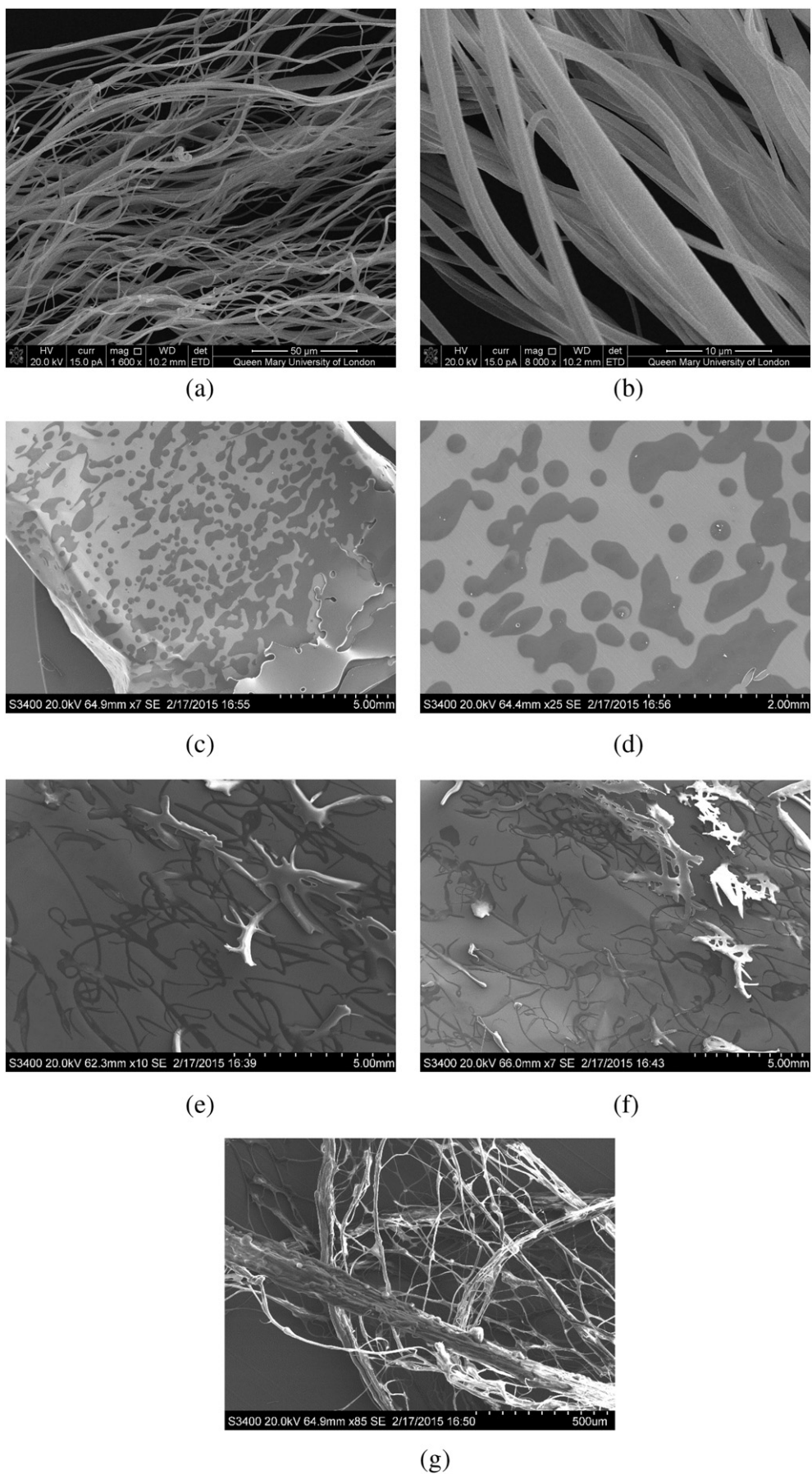


**Fig. 2.** SEM images of products generated by pressurised gyration at 36000 rpm and  $3 \times 10^5$  Pa (a) 5 wt% PAN (b) 15 wt% PAN (c) 15 wt% CA (d) 20 wt% CA (e), (f) 25 wt% CA (g) 10 wt% PAN-CA.

viscosity of the polymer solution that is being spun [18]. The measured values of surface tension and viscosity for PAN, CA and PAN-CA composite solutions are given in Table 1. It is apparent that the surface tension force of the polymer solutions increases with increasing polymer concentration. The surface tension values are higher for CA polymer solutions compared to PAN and PAN-CA polymer solutions. The viscosity values are higher for PAN solutions, an addition of CA polymer to PAN solutions does not significantly change the viscosity of the blend solutions. The viscosity of the CA solutions are low compared to other polymer solutions. It is worth noting that for a given polymer and solvent system, the change in surface tension due to change in concentration of the polymer solution is moderate, on the other hand the change in viscosity is significant. Several studies have been conducted to show the influence of surface tension and viscosity forces during forming, including pressurised gyration [15–19]. When the surface tension force is predominant over the viscosity forces beads or bead-on-string structures are formed. Formation of smooth, bead free fibres are promoted when the viscosity forces prevails over the surface tension force.

The SEM pictures of the fibres formed by pressurised gyration are showed in Fig. 2. For all concentrations of PAN solutions pore-free smooth fibres were generated by varying the rotating speed between 10,000 rpm to 36,000 rpm and varying the working pressure between  $1 \times 10^5$  Pa to  $3 \times 10^5$  Pa. Apparently, these fibres are without any artefacts such as beading and the fibre diameter varied between 200 and 500 nm. The fibre architecture of PAN appears homogeneous (Fig. 2a,b). CA solutions generated fibres at 25 wt% concentration. The fibre architecture of CA appears inhomogeneous and mostly contained short fibres (Fig. 2e,f). It could be deduced from the micrographs that their lengths varied between 1 and 3 mm compared to PAN fibres which are few centimetres long. In addition, an anisotropic distribution of fibre orientation was clearly seen in these fibres compared to an isotropic distribution of fibre orientation in PAN fibres. Moreover, there appears to be good bonding between the short fibres at most points of contact. Below 25 wt% concentration, CA polymer solution produced beads at all rotating speeds and working pressures. Interestingly, the beads had various morphologies (polygon shapes) largely due to surface tension and wetting effects of the substrate (Fig. 2c,d). The 10 wt% PAN-CA solution formed smooth fibres without any beading. A higher degree of fibre alignment was found on these fibres compared to CA fibres (Fig. 2g). The formed composite fibres are longer and the surface of the fibres appeared rougher than the PAN or CA fibres' morphologies. The fibre diameters varied between 500 and 2000 nm.

The TGA of the PAN-CA blended fibres is shown in Fig. 3. The fibre samples show two-stage degradation where a steep weight loss prevails to  $\sim 325$  °C and this is followed by another more gradual weight loss to

$\sim 400$  °C. The final solid residue corresponds to 74% of the initial weight. The initial weight loss is due to the solvent evaporation and dehydration. The second weight loss is associated with the carbonisation of the PAN molecules.

The nitrogen adsorption and desorption isotherm for the BET surface area analysis is shown in Fig. 4a. BET surface area plot is shown in Fig. 4b and the surface area determined is  $12 \text{ m}^2/\text{g}$ . The BET measurements showed a wide size distribution of pore size of the PAN-CA fibres with the pore size ranging from 7 to  $247\text{\AA}$  (Fig. 4c). Pore size can influence the contact angle of the polymer fibres. In addition, hydrophilic or hydrophobic groups within the polymer chain can determine the contact angle of the fibres. The hydrophilic nature of PAN-CA fibres and an accompanying wide range of pore size will have a huge impact on the wettability of the generated blended fibres.

It is well known that addition of another solvent to acetone causes variations in the diameter and morphology of the polymer fibres generated by spinning [25]. The addition of DMF to acetone - polylactic acid (PLA) polymer solutions produced the thinnest bead free fibres due to exertion of stronger elongation forces during a spinning process [25]. In fact, the solvent ratio in a binary acetone/DMF solvent system influenced PLA product formation and morphology. A ratio  $< 1:1$  did not generate any fibres. The optimum condition (that is defect free smooth thinnest fibres) were obtained with a solvent ratio 1.5:1. This is largely due to variation of viscosity and the surface tension of the solutions. In our work, a slightly higher ratio of 2:1 is found to be the optimum condition. A possible explanation for this difference could be that ambient conditions such as temperature and humidity varied during the gyration spinning process which may influence the morphology of the fibres. Moreover, in a mixed solvent system when the boiling point of the second solvent is higher than the first solvent, the fibre diameter and the morphology vary dramatically [26]. This is due to the solvent with the higher boiling point evaporating slowly from the ejected fibre jets during spinning and causing viscoelastic properties to change and hence the stretching of the fibre jets.

Another possible argument for variation of fibre morphologies in this work is the change in molecular weight of the polymers. It has been shown that change in molecular weight affects the fibre morphology [27]. In this work PAN has a higher molecular weight and CA has a lower molecular weight. Thus, the blend molecular weight can be dependent on the amount of each polymer present in the blend. There was a significant change in aspect ratio (fibre length/diameter) reported when decreasing the molecular weight of the polymer system [27]. In a spinning process, there must be a minimum molecular weight of polymer required to form sufficient chain entanglement which influence the formation of continuous bead free fibres [18]. In our work, CA polymer has lower molecular weight compared to PAN (thus having low chain entanglement) that led to dramatic change in fibre morphology. The current knowledge of molecular chain length, chain conformation, degree of chain entanglement and extensional rheology with respect to pressurised gyration to relate the fibre morphology and aspect ratio is not complete, although it has been shown that a critical solution concentration is needed to form continuous fibres in this process [18–21]. Thus, this study describes a partial qualitative assessment on how those parameters could affect the fibre morphology and the aspect ratio of fibres formed by pressurised gyration.

### 3.2. Porous fibre formation

Fig. 5 shows the high and low magnification SEM images of the PAN-CA fibre morphologies generated at different working pressures and a fixed rotating speed 36,000 rpm. It is clearly seen that the fibre assembly exhibited extensive bundles consisting of many fibres that stuck together. They are also longer and thicker than the fibres produced from PAN and CA alone. It is also noteworthy that the fibre samples have a distinct layered structure made up of several fibres stacked together in the upper and lower regions of the micrographs. This is a

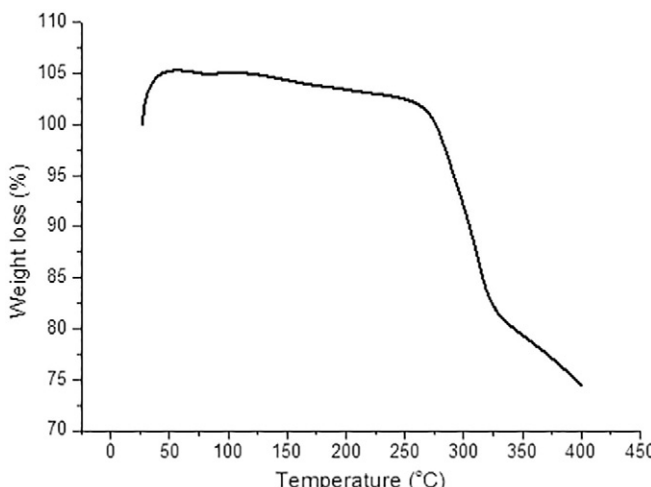
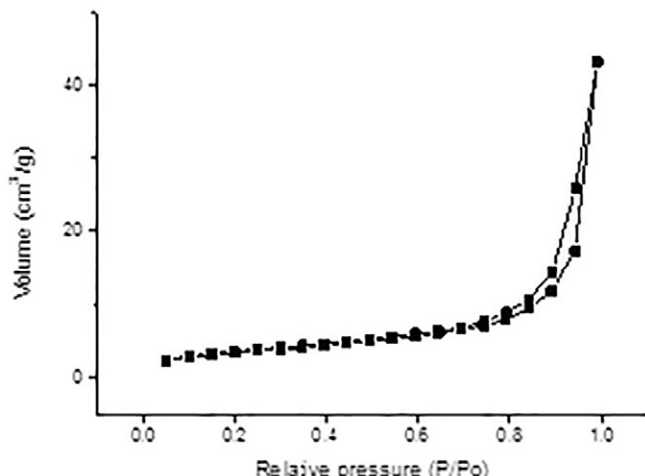
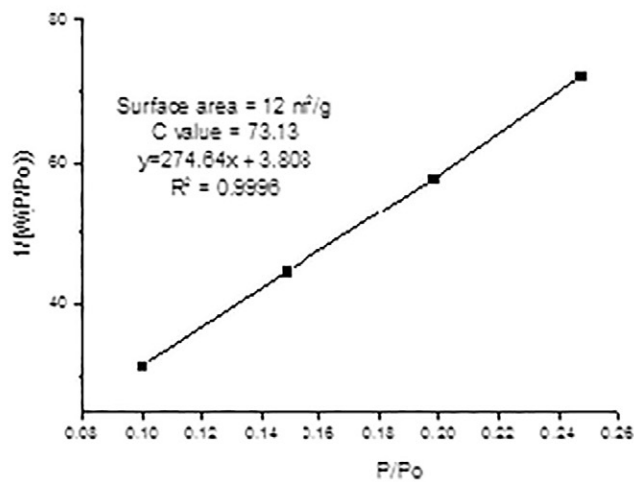


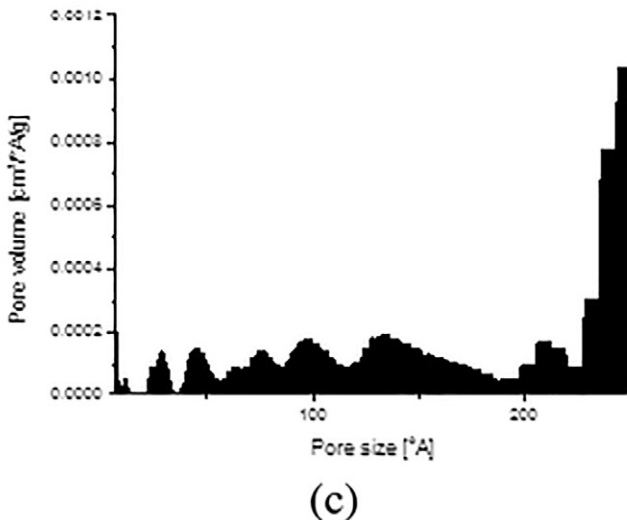
Fig. 3. Experimental TGA curve for the PAN-CA blended fibres.



(a)



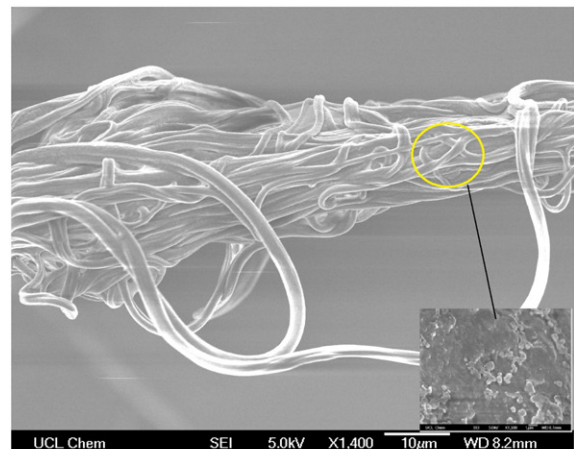
(b)



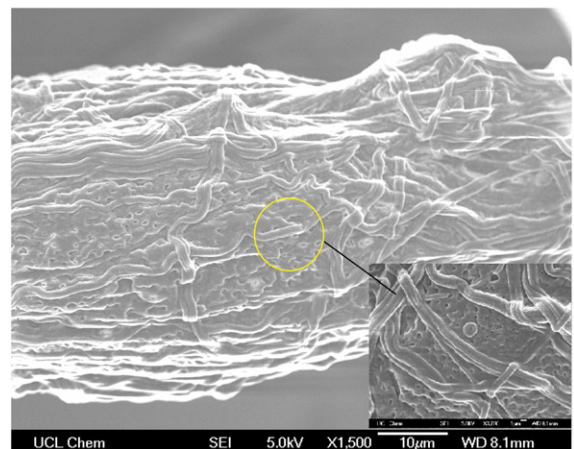
(c)

**Fig. 4.** (a) Nitrogen adsorption-desorption isotherm (b) BET surface area plot (c) pore size distribution plot from BET measurement. W is the work function of  $P/P_0$ .

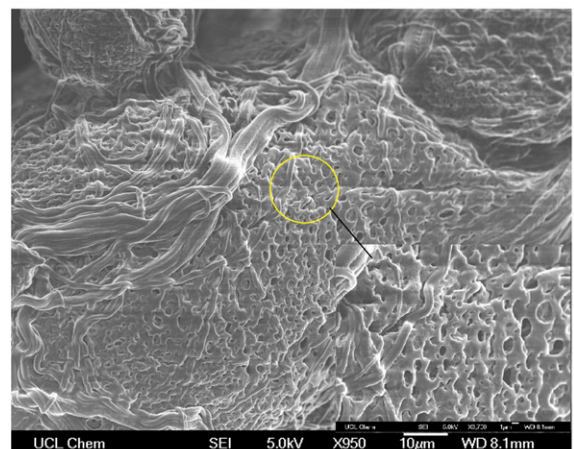
very distinguishable feature of the PAN-CA fibres compared to only PAN and only CA fibres (Fig. 2a,c). Another remarkable observation of these blend fibres is their ability to generate pores on their own



(a)



(b)



(c)

**Fig. 5.** High and low magnification SEM images of PAN-CA blended fibres generated by pressurised gyration at 36000 rpm and at different working pressures. (a)  $1 \times 10^5$  Pa (b)  $2 \times 10^5$  Pa (c)  $3 \times 10^5$  Pa.

without any additives or post-processing. At a rotating speed 36,000 rpm and a working pressure  $1 \times 10^5$  Pa there are no pores on the surface of fibres (Fig. 5a). However, increasing the working pressure from  $1 \times 10^5$  Pa to  $2 \times 10^5$  Pa at the same rotating speed generated pores on the surface of fibres (Fig. 5b). This is also true when increasing the

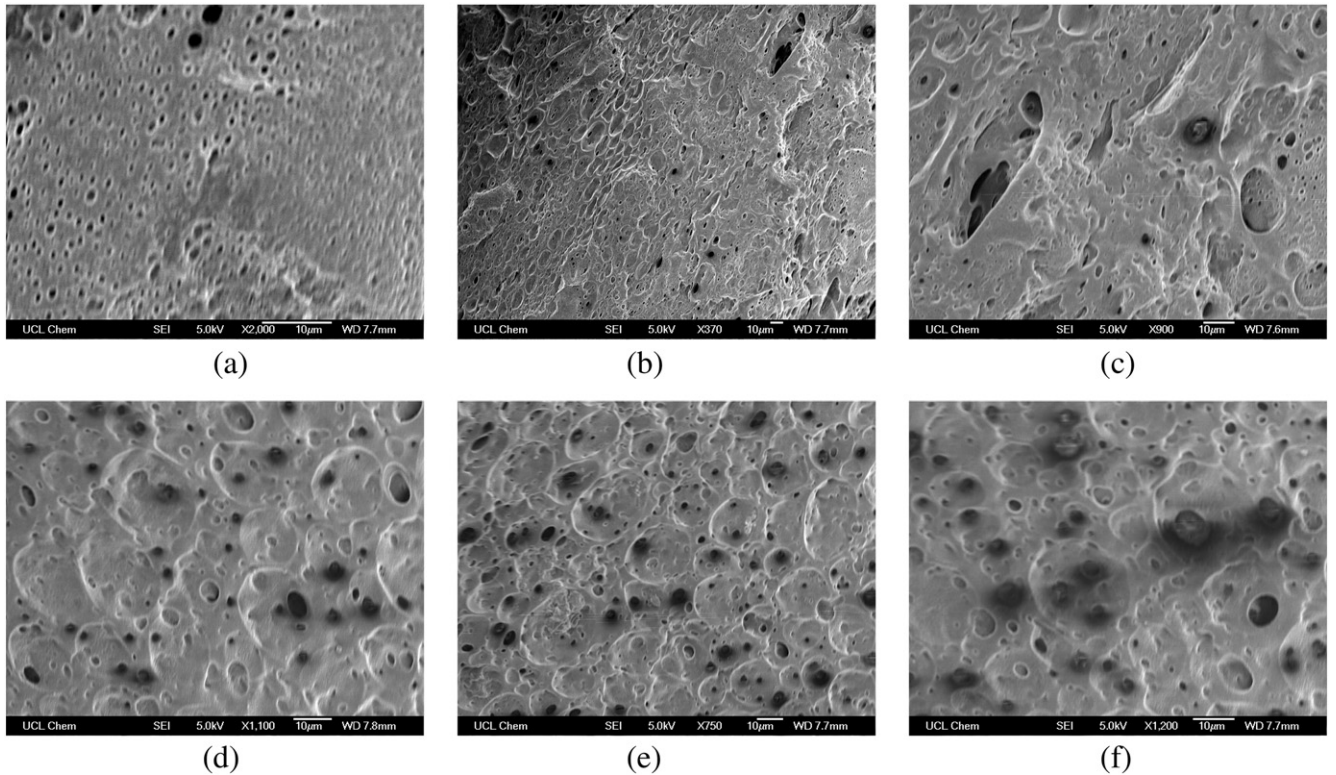


**Fig. 6.** PAN-CA fibre microstructures generated by pressurised gyration at 36000 rpm and after solvent etching: (a) 5 (b) 10 (c) 15 (d) 20 (e) 25 (f) 30 min.

working pressure from  $1 \times 10^5$  Pa to  $3 \times 10^5$  Pa at the same rotating speed but the incidence of pores is much higher than under the previous conditions (compare Fig. 5b with Fig. 5c).

For comparative purposes we have also generated porous fibres using particulate (NaCl) leaching and the solvent etching processes. Fig. 6 shows fibre morphologies of the composites after etching in

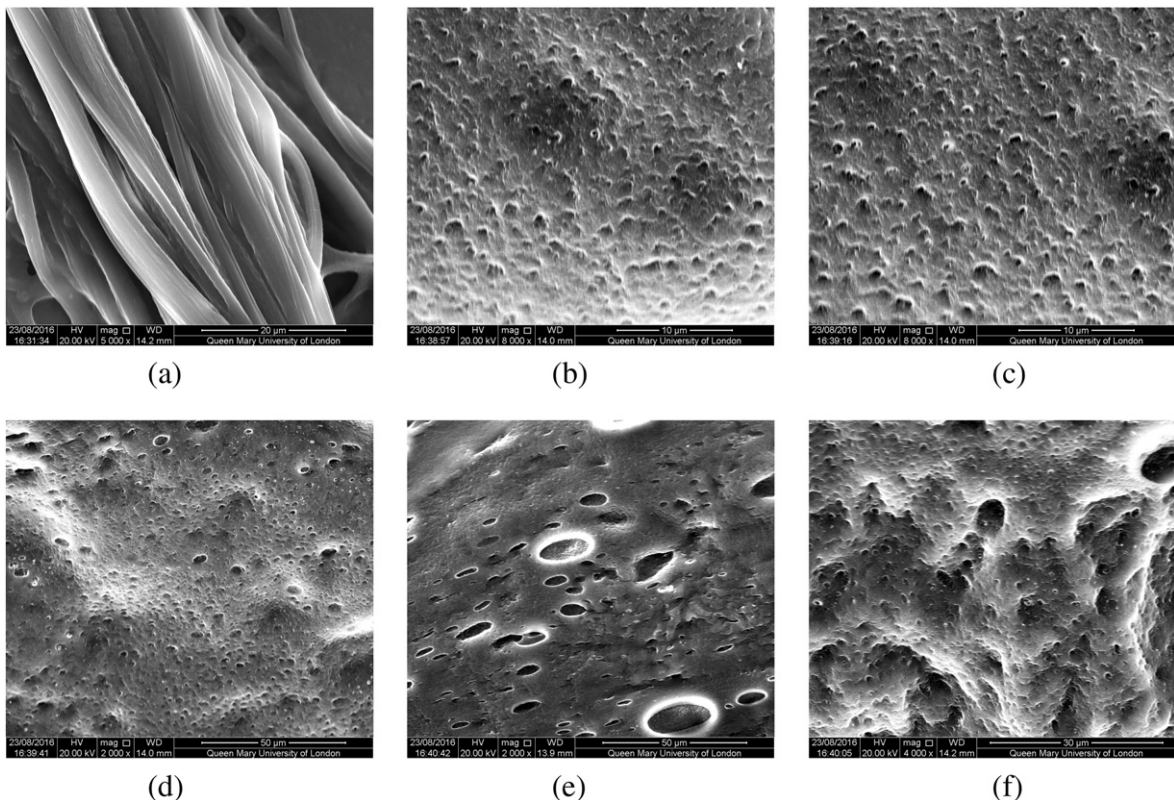


**Fig. 7.** PAN-CA fibre microstructures generated by pressurised gyration at 36000 rpm and after NaCl leaching, porogen concentration (wt%) (a) 0 (b) 0.2 (c) 0.4 (d) 0.6 (e) 0.8 (f) 1.

acetone/DMF solution for various time intervals ranging from 5 to 30 min. It is apparent that the fibres were dissolved in the solution leaving imprints on the surface of the fibres. The pore sizes gradually increased with etching time. It is also noteworthy that at higher etching times there is pitting on fibre surfaces and the pores extended deep into the fibre matrix. The porous fibre structures generated with NaCl leaching are shown in Fig. 7. There were no pores obtained in the absence of porogen NaCl. However, in contrast, when porogen was present pores formed on the surface of these fibres. The pore size increased with the concentration of porogen. Also, the absence of NaCl crystals on the surface suggests that the dissolution of the porogen crystals is complete. Fig. 8 shows pore size variation as a function of the key variables of each fibre forming route. In the self-generating route, increasing the working pressure from  $2 \times 10^5$  Pa to  $3 \times 10^5$  Pa caused a twofold increase in pore size from 0.5 to 1.2  $\mu\text{m}$ . In the etching process, the pore size increased dramatically for the first 15 min, thereafter the rate of increase was reduced even though the pore size increased with time. Finally, in the porogen leaching process the pore size increased with the concentration of porogen NaCl. There was a gradual increase in pore size up to 0.4 wt% NaCl, then it levelled off to 0.6 wt%, subsequently gradual increase was prevalent again. However, the rate of increase was lower than that was observed at the lower concentration of NaCl.

It is important to quantitatively assess the overall pore size variation after each preparation method. For that we have mapped the pore size distribution for each case and found out the statistical importance with Gaussian plots. The pore size distribution of the PAN-CA fibrous samples prepared under different conditions is shown in Fig. 9. As expected increasing the working pressure increased the pore size in the self-generating fibrous structures. The pore size showed unimodal distribution with a peak showing a mean value  $\sim 0.5 \mu\text{m}$  for  $2 \times 10^5$  Pa and  $\sim 1.3 \mu\text{m}$  for  $3 \times 10^5$  Pa working pressures. Unimodal pore size distribution is also obtained in the other two preparation techniques. The etching method showed a mean value  $\sim 0.5 \mu\text{m}$  and  $9.5 \mu\text{m}$  after 5, 30 min etching time, respectively. The standard deviation of the former is smaller than the standard deviation of the latter confirming the qualitative assessment that the pore size gets larger with increasing etching time. In the case of particulate leaching the pore size is mostly populated at  $\sim 1.3 \mu\text{m}$  and  $\sim 4.5 \mu\text{m}$  for NaCl concentrations of 0.2 wt% and 1 wt%, respectively. All these results imply that the variables of the processing techniques greatly influence the pore size and its distribution. To study the influence of NaCl particle size on the pore size and pore size distribution, we have also evaluated the NaCl particle size distribution which is shown on Fig. 10. The NaCl particle size shows a unimodal distribution with a mean value  $\sim 185 \mu\text{m}$ . This is significantly lower than the pore size obtained in the particle leaching method. In fact, it is two orders of magnitude less than the pore size of all the preparation techniques. The chronological argument for this observation is that the volume fraction of particles that are higher in dimension ( $>10 \mu\text{m}$ ) might be suspended and segregated during the spinning process or might be largely present on the surface of fibres generated and are easily eroded away during leaching. The smaller volume fraction of particles that have size  $<10 \mu\text{m}$  could have occupied the space between the interstices of the polymer chains which can only erode away after deep leaching and this could have a more significant effect the observed results compared with the influence of the  $>10 \mu\text{m}$  particles. To evaluate the amount of residual NaCl chloride particles that were entrapped in the fibres, the concentration of the chloride particles were determined. In all instances the concentration of chloride ion was  $<10 \text{ ppm}$  which represents  $\sim 0.0006 \text{ wt\%}$  of total mass fraction of the NaCl added into the fibres.

The self-generating porous nature of the blend fibres is intriguing and its formation mechanism deserves more attention. The high volatility and vapour pressure solvents give rise to phase separation and surface porosity in formed fibres. The porosity and smoothness of the surface of the fibres could be manipulated by decreasing solvent

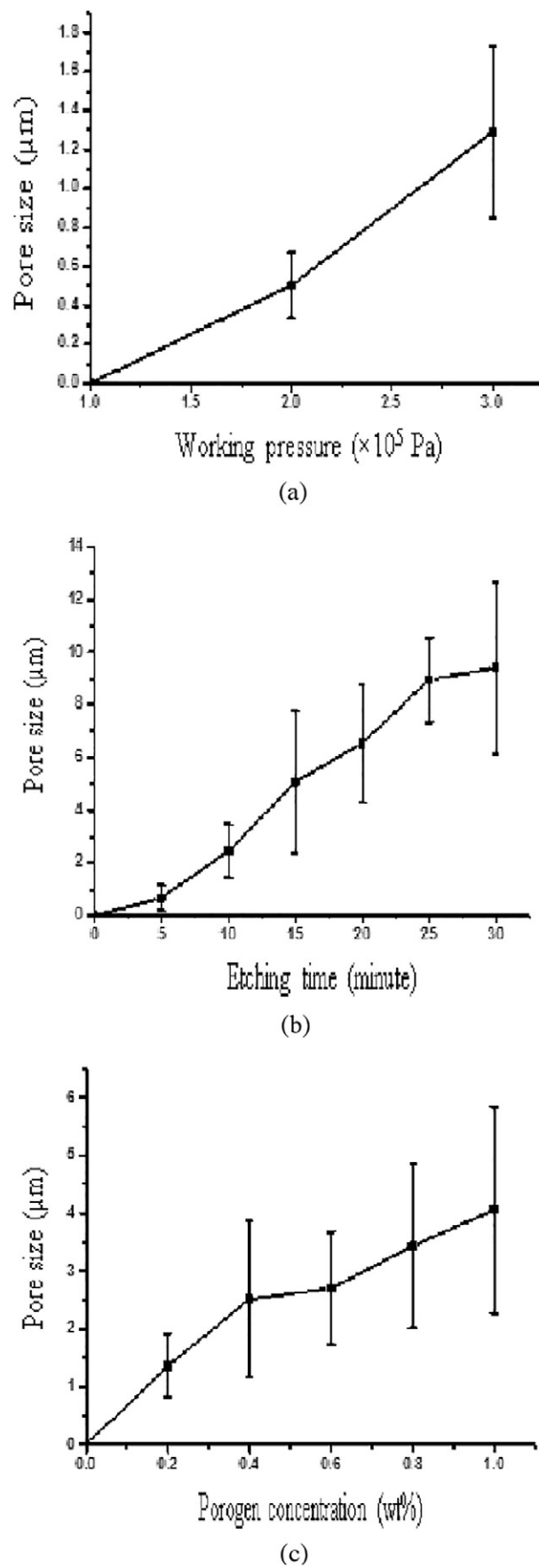


**Fig. 8.** Pore size variation in PAN-CA porous fibres: (a) self-generating (b) etched (c) porogen leached.

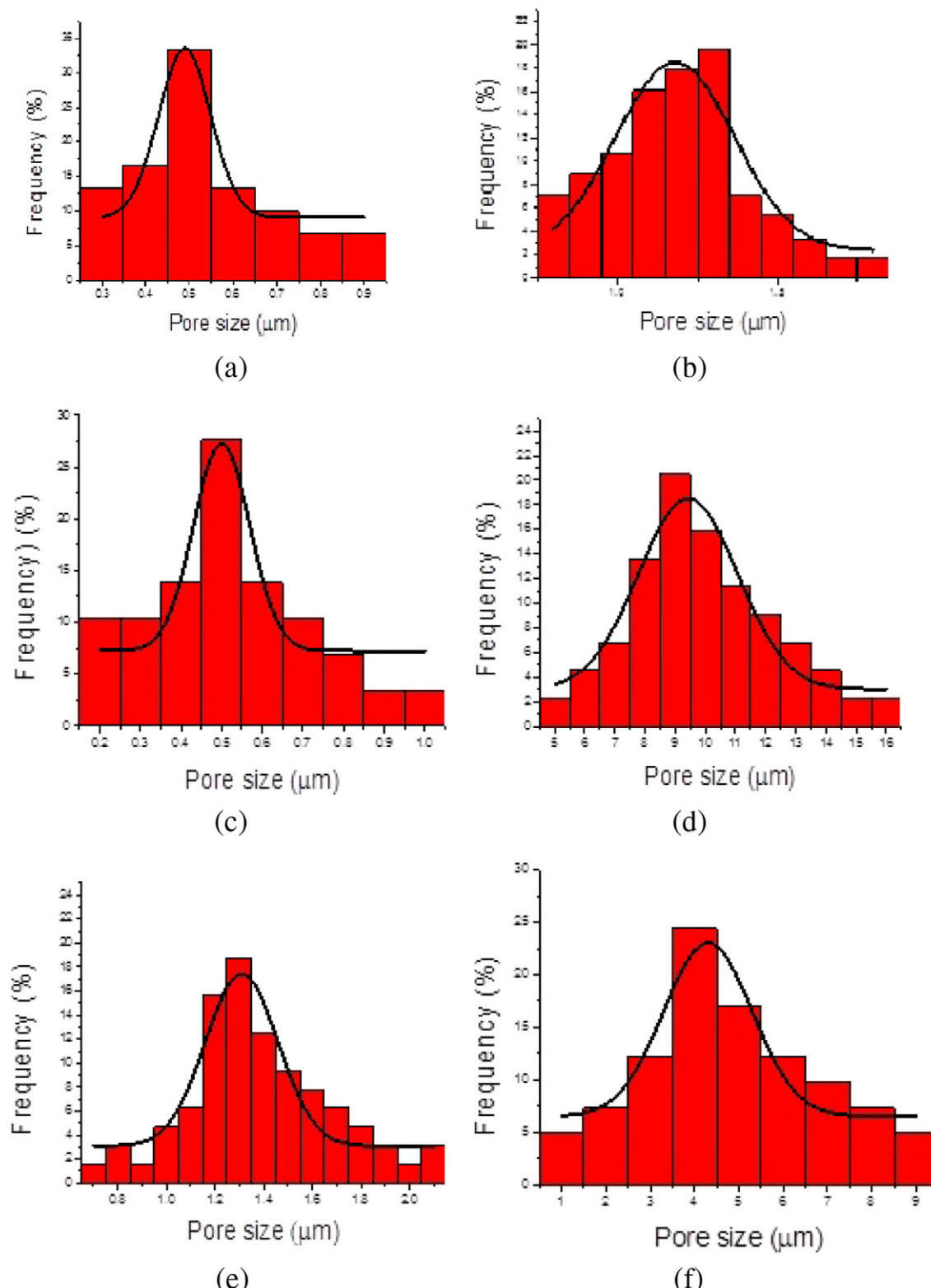


**Fig. 9.** Pore size distribution in PAN-CA porous fibres: (a), (b) self-generating at  $2 \times 10^5$  Pa and  $3 \times 10^5$  Pa working pressure (c), (d) etched after 5, 30 min (e), (f) porogen leached with 0.2 and 1 wt% NaCl.

volatility [28]. During the stretching and cooling process in fibre formation, the evaporation rates of the solvents vary in the binary solvent system which contain different boiling point solvents. The rapid evaporation of the more volatile solvent (in this case acetone) can lower the temperature of the liquid jet by absorbing heat. This leads to a solvent-rich phase and a polymer-rich phase, eventually the latter

transforms into a solid matrix and the former evaporates to leave pores in the matrix. Another plausible explanation is that the non-solvent of polymer systems such water vapour in the atmosphere condenses and diffuses in to the polymer matrix to leave imprints on the surface. This is because of the evaporative cooling of the solvents, thus there is more saturated environment during spinning and it is more

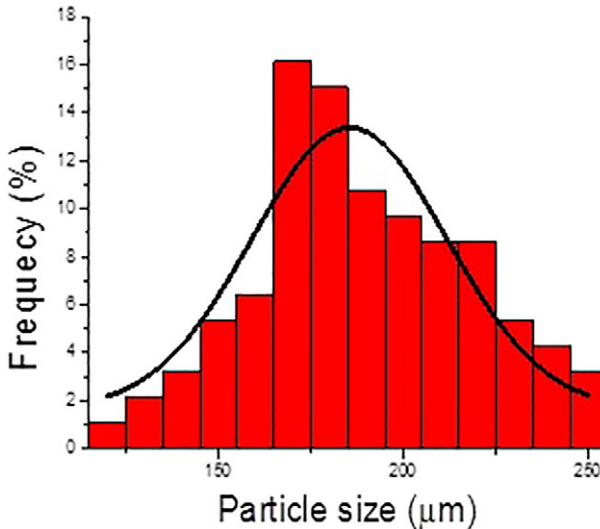


Fig. 10. Particle size distribution of NaCl crystals.

probable that the dew point of water is reached [29]. During the etching process the polymer molecules dissolve in the “good” solvent and selective removal of the polymer phase leads to pore formation. As the etching time increases the polymer molecules beneath the surface of the blend fibres are more exposed to solvent molecules and this increases the interaction between these molecules, this will facilitate pitting on the matrix. On the contrary, in the leaching process the selective removal of the porogen NaCl generated pores in the matrix. In this process porosity is governed by the amount of leachable particles present in the polymer matrix whereas pore size and shape of the generated structure can be tailored independent of the porosity by varying the characteristics of the particles such as size and shape [30]. Moreover, the inter-connectivity of the pores mostly depends on the spatial arrangement of particles in the matrix. Therefore, higher the concentration of the particles the higher the inter-connectivity and vice-versa.

### 3.3. Mathematical modelling

The formation of self-generated porous fibrous structures is mainly due to solvent evaporation and change in solvent evaporation rate during the pressurised gyration of polymer solution. For deriving a mathematical model we consider a time scale where fibre has ejected from the orifice and is sufficiently stretched in axial direction. As gyration is carried out in a sealed vessel, we assume solvent evaporation takes place at this point, therefore, the solvent evaporation rate (i.e. the mass transfer rate of solvent from the surface of the fibre jet) could be related to diffusion of solvent atoms from the surface of the fibre jet. The surface mass concentration near the fibre jet  $C$  can be related to the diffusion coefficient by:

$$V_x \frac{\partial C}{\partial x} = D \frac{\partial^2 C}{\partial y^2} \quad (1)$$

where, the  $x$ -axis is tangential to the local surface and the  $y$ -axis is perpendicular to the local surface,  $V_x$  is the tangential air flow speed relative to the fibre jet,  $D$  is the solvent diffusion constant.

The length scale of mass diffusion  $L$  near the local surface can be expressed as:

$$V_x \frac{C}{L_x} = D \frac{C}{L_y^2} \quad (2)$$

Therefor the length scale of mass diffusion  $L_y$  is

$$L_y = \sqrt{\frac{DL_x}{V_x}} \quad (3)$$

Now we consider the rotational and blowing frames to derive the length scale of mass diffusion  $L_y$  in pressurised gyration forming. In the rotational frame, only the rotating action of the process is considered. Therefore,  $V_x$  could be related to angular speed  $\omega$  and the radius of the gyration vessel  $R$  by,

$$V_x = \omega R \quad (4)$$

$L_x$  is radius of the fibre jet  $r$ . That will give the length scale of mass diffusion in the rotating frame:

$$L_y = \sqrt{\frac{Dr}{\omega R}} \quad (5)$$

In the blowing frame, only blowing action of the process is considered. Therefore,  $V_x$  can be related to the aerodynamic drag force acting on the fibre jet  $q$  and the density of the gas  $\rho$  and the cross-sectional area  $m^2$ .

$$V_x = \sqrt{\frac{q}{\rho \pi r^2}} \quad (6)$$

This will give the length scale of mass diffusion in blowing frame as:

$$L_y = \sqrt{\frac{Dr}{\sqrt{\left(\frac{q}{\rho \pi r^2}\right)}}} \quad (7)$$

The flux of surface mass transfer ( $J$ ) can be given by

$$J = \frac{DC_a}{L_y} \quad (8)$$

where  $C_a$  is the solvent vapour concentration in air near the fibre jet. By substituting from Eqs. (5) and (7) for  $L_y$ , the flux of surface mass transfer in rotating and blowing frames could be obtained. This will give the flux of surface mass transfers for rotating frame  $J_R$  and the blowing frame  $J_B$  as follows.

$$J_R = \frac{DC_a}{\sqrt{\frac{Dr}{\omega R}}} = C_a \sqrt{\frac{D\omega R}{r}} \quad (9)$$

$$J_B = \frac{C_a}{r} \sqrt{D \sqrt{\frac{\rho \pi}{q}}} \quad (10)$$

The solvent mass evaporation rate was determined experimentally by evaporating the solvents DMF and acetone/DMF mixtures over a period of time. They were found to be 0.15 g/min and 0.20 g/min respectively. Substituting values for angular speed  $\omega = 36,000$  rpm, radius of the gyration vessel  $R = 60$  mm, diffusion constant =  $0.276 \text{ cm}^2/\text{s}$  [31], the radius of the fibre jet at the rotational frame would be 600 nm. Assuming density of air  $\rho = 1.225 \text{ kg m}^{-3}$ , the radius of the fibre jet at the blowing frame would be 800 nm. This value is within the range of fibre diameter obtained in experiments, i.e. 200–2000 nm.

### 3.4. Bonding characteristics of gyrated fibres

FTIR was used to investigate the changes in chemical bonding on the surface of fibres after pressurised gyration. Fig. 11a shows, FTIR spectra

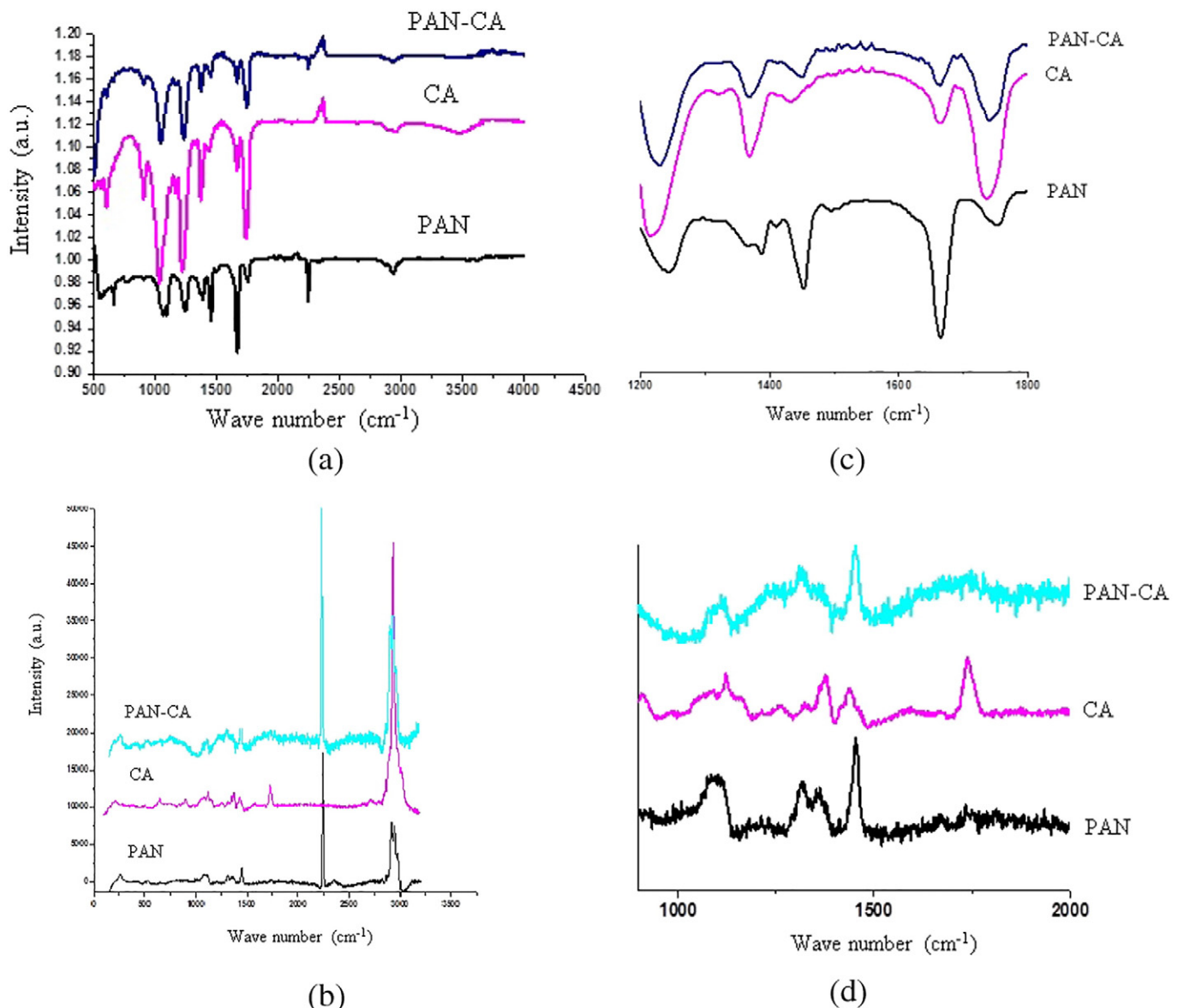


**Fig. 11.** (a) FTIR and (b) Raman spectra of the different fibres prepared in this work. a.u. indicates arbitrary units. (c), (d) highly resolved spectra of FTIR and Raman data, relevant to (a) and (b), respectively.

of the gyrate PAN, CA and PAN-CA fibres obtained at a rotating speed 36,000 rpm and  $3 \times 10^5$  Pa working pressure. For PAN fibres, the C≡N stretching mode was found at 2247 cm<sup>-1</sup>. The -CH<sub>2</sub> bending peak was obtained at 1455 cm<sup>-1</sup> [32]. The -CH<sub>2</sub> vibrational mode was attained at 2940 cm<sup>-1</sup> [33]. Additionally, there is a peak at 1074 cm<sup>-1</sup> which is attributed to S=O bond arising from solvent DMF. The characteristic chemical bonding peaks for CA fibres were found at 1740, 1365 and 1216 cm<sup>-1</sup> for ester carbonyl (C = O), carbon methyl (CCH<sub>3</sub>) and ester linkage (OC = O), respectively [34]. The PAN-CA fibres showed all the peaks found on individual PAN and CA fibres suggesting that well-blended fibrous structures were made by pressurised gyration. To prove this we have also carried out Raman spectroscopy on the gyrate fibres. Fig. 11b shows the Raman spectra of all fibres formed at 36000 rpm and  $3 \times 10^5$  Pa working pressure. The Raman scattering of nitrile group (-CN) appeared at 2245 cm<sup>-1</sup>. The C—H deformation peak was obtained at 1103 cm<sup>-1</sup>. The -CH bonds were attained at 2917 cm<sup>-1</sup>. The methyl (-CH<sub>3</sub>) group was obtained at 1455 cm<sup>-1</sup>. Raman spectra of cellulose acetate show characteristics bands at 1095, 1376 and 1748 cm<sup>-1</sup> corresponding to C—O rings and glycosidic linkage stretching, methyl group and -C=O vibrational bonds,

respectively [35,36]. The chemical bonding, change in chemical bonding and the frequency shift are identified in the obtained spectra by zooming in the frequency range 1200–1800 cm<sup>-1</sup> for FTIR and 900–2000 cm<sup>-1</sup> for Raman spectroscopy, as shown in Fig. 11c and d, respectively.

### 3.5. Release characteristics of vanillin from porous fibrous structures

Fig. 12 shows release characteristics of the porous structures as a function of time and temperature. It can be seen that the release of vanillin from the fibres can be related to the porous structures. Self-generated porous structures shows higher release compared to etched and leached porous fibrous structures. The release of vanillin in these structures is rapid when increasing the temperature from 20 °C to 100 °C. In fact, more release is seen much sooner. Etched porous structures shows a slight increase in release compared to leached porous structures. Again, increasing the temperature increased the amount of vanillin released. A two stage release is observed for self-generated and etched porous structures, while leached porous structures showed a linear release profile. The change in release

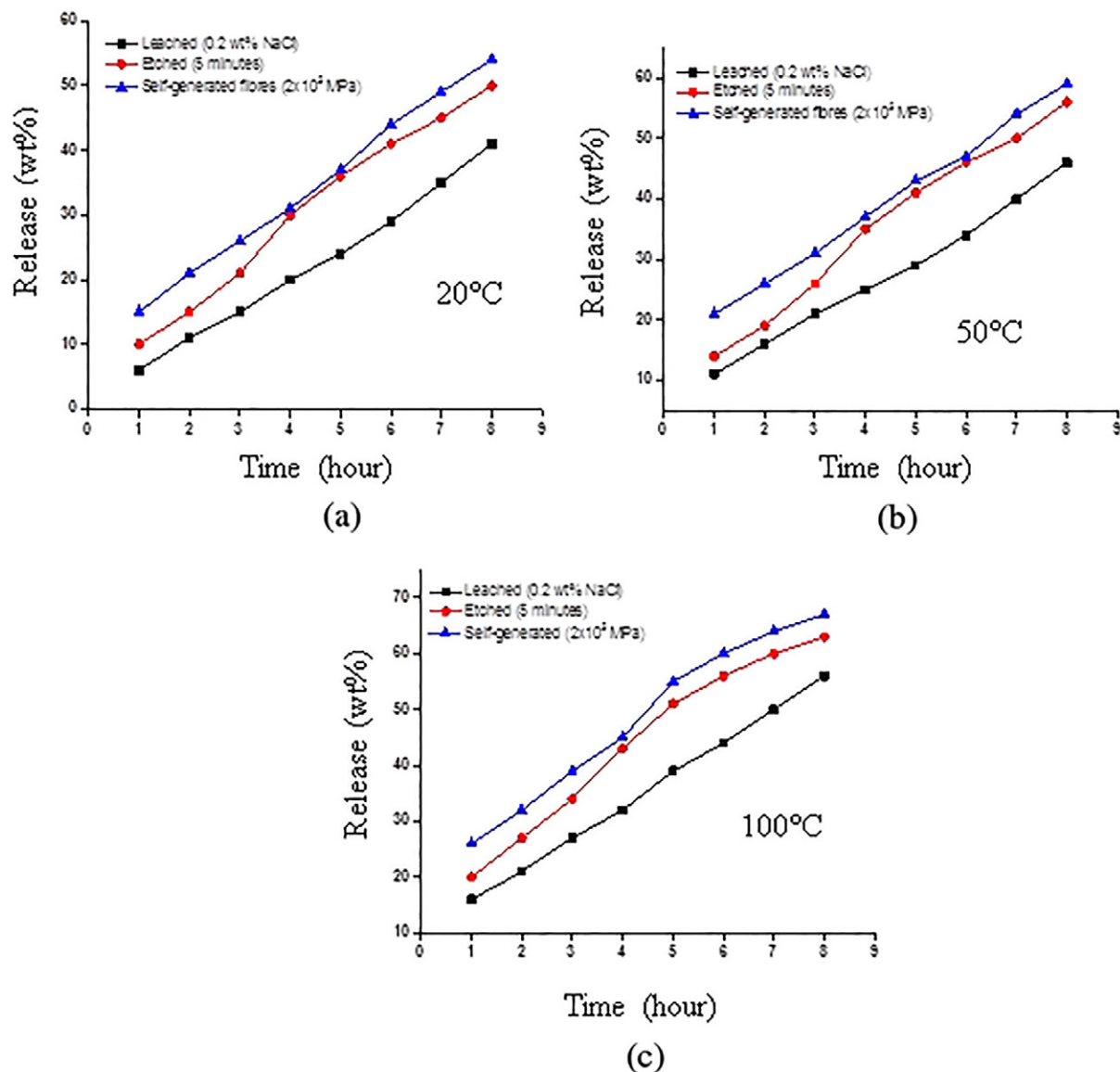


**Fig. 12.** Release characteristics of vanillin from porous fibrous structures at various temperatures. (a) 20 °C (b) 50 °C (c) 100 °C.

characteristics could be attributed to their different pore size and morphologies. The self-generated structures have finer pores than the etched and leached structures. The pore size is lower in the following order: Self-generating (0.5 µm) < etched (0.7 µm) < leached (1.4 µm). The finer pores give more surface area for attachment of the vanillin molecules and their release in a given medium. In the leached structures, the pores are well open and have long channels that might slow down the diffusion process. In addition, there may be stronger residual ionic components present in the form of Na<sup>+</sup> and Cl<sup>-</sup> ions that will attract these vanillin molecules strongly. This will prevent them from diffusing easily through the inter-connected structures. Therefore, we believe that these factors contribute to a lower release rate in the leached porous structures. Another striking observation is that the release of vanillin is not saturated within the time of investigation. The release can be categorised into release from open pores and solid state diffusion. The manifestation of these facts is that saturation will be reached when the solid state diffusion is complete which is a slow process and incommensurate with the overall duration of the release experiments. To evaluate the effect of temperature on the release characteristics we have plotted Higuchi (based on Fickian

diffusion mechanism) model release data profile using the following equation,

$$Q = K_H t^{1/2} \quad (11)$$

The best R<sup>2</sup> value and the Higuchi constant K<sub>H</sub> is tabulated in Table 4. All coefficient of determination are above 95% indicating the excellent fit to the proposed model.

The temperature dependent increase in dye release from the porous fibrous structures is attributable to two factors. Firstly, as the temperature increases the swelling of the fibrous structures increase. This is

**Table 4**  
Higuchi model (Eq. (11)) fit of the release data profiles.

Sample	25 °C		50 °C		100 °C	
	R <sup>2</sup>	K <sub>H</sub>	R <sup>2</sup>	K <sub>H</sub>	R <sup>2</sup>	K <sub>H</sub>
Leached (NaCl)	0.96	11.69	0.98	15.81	0.99	17.35
Etched (5 min)	0.98	14.00	0.99	18.08	0.99	19.62
Self-generated (2 × 10 <sup>5</sup> Pa)	0.99	17.84	0.99	21.98	0.99	23.82

mainly due to increased attraction between hydrophobic segments of the polymers and the weakening of the hydrogen bonding between the water molecules and the hydrophilic segments of the polymers [37]. Thus, it could facilitate the escape of dye molecules from its surface. Secondly, as the temperature increases the drug molecules gain sufficient kinetic energy which could overcome the bonding between its molecular surface and fibre surface.

#### 4. Conclusions

In the present work, simple and versatile fabrication of single and blended polymeric fibres was achieved with various fibre morphologies and surface properties. It is shown that by controlling working pressure in the pressurised gyration process, self-generating porous structures could be obtained. Artificial porous fibrous structures were also made by post-processing leaching and etching. The pore size was controlled by adjusting the processing variables for each case and the pore formation mechanisms were elucidated for each processing route. A mathematical model was formulated to relate the solvent mass transfer with respect to processing parameters and the fibre jet radius. Chemical bonding characteristics in the fibres were studied with spectroscopy techniques suggesting that good quality blended fibres were generated by pressurised gyration. We have also demonstrated the release characteristics of vanillin molecules from the porous structures in de-ionised water at various temperatures. The release characteristics of the self-generated porous structures is more pronounced compared to etched and leached porous structures.

Supplementary data to this article can be found online at <http://dx.doi.org/10.1016/j.matdes.2017.07.050>.

#### Acknowledgement

The authors are like to thank Engineering and Physical Sciences Research Council (EPSRC), UK for providing the financial support for the exploitation of pressurised gyration research (EP/L 023059/1 and EP/N 034228/1). Data supporting this study are provided in the paper and supplementary information.

#### References

- [1] H. Hou, L. Wang, F. Gao, G. Wei, J. Zheng, B. Tang, W. Yang, Hierarchically porous  $\text{TiO}_2/\text{SiO}_2$  fibers with enhanced photocatalytic activity, *RSC Adv.* 4 (2014) 19939–19944.
- [2] C.-K. Hsieh, M.-C. Tsai, M.-Y. Yen, C.-Y. Su, K.-F. Chen, C.M. Ma, F.-R. Chen, C.-H. Tsai, Direct synthesis of platelet graphitic-nanofibres as a highly porous counter electrode in dye-sensitised solar cells, *Phys. Chem. Chem. Phys.* 4 (2012) 4058–4061.
- [3] S. Cavaliere, S. Subianto, I. Savych, D.J. Jones, J. Roziere, Electrospinning: designed architectures for energy conversion and storage devices, *Energy Environ. Sci.* 4 (2011) 4761–4785.
- [4] L. Yin, Y. Chen, D. Li, X. Zhao, B. Hou, B. Cao, 3-Dimensional hierarchical porous activated carbon derived from coconut fibers with high-rate performance for symmetric supercapacitors, *Mater. Des.* 111 (2016) 44–50.
- [5] H.R. Pant, M.P. Neupane, B. Pant, G. Panthi, H.-J. Oh, M.H. Lee, H.Y. Kim, Fabrication of highly porous poly( $\epsilon$ -caprolactone) fibres for novel tissue scaffold via water bath electrospinning, *Colloids Surf. B* 88 (2011) 587–592.
- [6] H.-M. Yin, X. Li, Y.-Z. Xu, B. Zhao, J.-H. Li, Z.-M. Li, Highly aligned and interconnected porous poly( $\epsilon$ -caprolactone) scaffolds derived from co-continuous polymer blends, *Mater. Des.* 128 (2017) 112–118.
- [7] K.A.G. Katsogiannis, G.T. Vladisavljevic, S. Georgiadou, Porous electrospun polycaprolactone (PCL) fibres by phase separation, *Eur. Polym. J.* 69 (2015) 284–295.
- [8] S.C. Moon, J.K. Choi, R.J. Farris, Highly porous polyacrylonitrile/polystyrene nanofibres by electrospinning, *Fibre. Polym.* 9 (2008) 276–280.
- [9] M. Mehraban, A. Zadhoush, S.A.H. Ravandi, R. Bagheri, A.H. Tehrani, Preparation of porous nanofibers from electrospun polyacrylonitrile/calcium carbonate composite nanofibers using porogen leaching technique, *J. Appl. Surf. Sci.* 128 (2013) 926–933.
- [10] M. Srinivasarao, D. Collings, A. Philips, S. Patel, Three-dimensionally ordered array of air bubbles in a polymer film, *Science* 292 (2001) 79–83.
- [11] T. Hou, X. Li, Y. Lu, B. Yang, Highly porous fibers prepared by centrifugal spinning, *Mater. Des.* 114 (2017) 303–311.
- [12] E.A. Morris, M.C. Weisenberger, M.G. Abdallah, F. Vautard, H. Grappe, S. Ozcan, F.L. Paulauskas, C. Eberle, D. Jackson, S.J. Mecham, A.K. Naskar, High performance carbon fibers from very high molecular weight polyacrylonitrile precursors, *Carbon* 101 (2016) 245–252.
- [13] J. Liu, H. Yue, H. Fong, Continuous nanoscale carbon fibers with superior mechanical strength, *Small* 5 (2009) 536–542.
- [14] H. Bi, G. Sui, X. Yang, E. Dickinson, Microstructure and mechanical properties of twisted carbon nanofiber bundles developed from impregnated electrospun polyacrylonitrile films, *RSC Adv.* 3 (2013) 20412–20421.
- [15] C. Huang, Y. Tang, X. Liu, A. Sutti, Q. Ke, X. Mo, X. Wang, Y. Morsi, T. Lin, Electrospinning of nanofibres with parallel line surface texture for improvement of nerve cell growth, *Soft Matter* 7 (2011) 10812–10817.
- [16] L. Wang, M. Wang, P.D. Topham, Y. Huang, Fabrication of magnetic drug-loaded polymeric composite nanofibres and their drug release characteristics, *RSC Adv.* 2 (2012) 2433–2438.
- [17] D.-G. Yu, X.-Y. Li, X. Wang, W. Chian, Y.-Z. Liao, Y. Li, Zero-order drug release cellulose acetate nanofibres prepared using coaxial electrospinning, *Cellulose* 20 (2013) 379–389.
- [18] S. Mahalingam, M.J. Edirisinghe, Forming of polymer nanofibres by a pressurised gyration process, *Macromol. Rapid Commun.* 34 (2013) 1134–1139.
- [19] S. Mahalingam, B.T. Raimi-Abraham, D.Q.M. Craig, M. Edirisinghe, Solubility-spinnability map and model for the preparation of fibres of polyethylene (terephthalate) using gyration and pressure, *Chem. Eng. J.* 280 (2015) 344–353.
- [20] S. Mahalingam, G.G. Ren, M. Edirisinghe, Rheology and pressurised gyration of starch and starch-loaded polyethylene oxide, *Carbohyd. Polym.* 114 (2014) 279–287.
- [21] S. Mahalingam, G. Pierin, P. Colombo, M. Edirisinghe, Facile one-pot formation of ceramics fibres from preceramic polymers by pressurised gyration, *Ceram. Int.* 41 (2015) 6067–6073.
- [22] B.T. Raimi-Abraham, S. Mahalingam, M. Edirisinghe, D.Q.M. Craig, Generation of poly(*N*-vinylpyrrolidone) nanofibres using pressurised gyration, *Mater. Sci. Eng., C* 39 (2014) 168–176.
- [23] S. Mahalingam, B.T. Raimi-Abraham, D.Q.M. Craig, M. Edirisinghe, Formation of protein and protein-gold nanoparticle stabilised microbubbles by pressurised gyration, *Langmuir* 31 (2014) 659–666.
- [24] S. Mahalingam, Z. Xu, M. Edirisinghe, Antibacterial activity and biosensing of PVA-lysozyme microbubbles formed by pressurized gyration, *Langmuir* 31 (2015) 9771–9780.
- [25] R. Casasola, N.L. Thomas, A. Trybala, S. Georgiadou, Electrospun poly lactic acid (PLA) fibres: effect of different solvent systems on fibre morphology and diameter, *Polymer* 55 (2014) 4728–4737.
- [26] L. Wannatong, A. Sirivat, P. Supaphol, Effects of solvents on electrospun polymeric fibers: preliminary study on polystyrene, *Polym. Int.* 53 (2004) 1851–1859.
- [27] C.J. Luo, E. Stride, S. Stoyanov, E. Pelan, M. Edirisinghe, Electrospinning short polymer micro-fibers with average aspect ratios in the range of 10–200, *J. Polym. Res.* 18 (2011) 2515–2522.
- [28] S. Megelski, J.S. Stephens, D.B. Chase, J.F. Rabolt, Micro-nanostructured surface morphology on electrospun polymer fibres, *Macromolecules* 35 (2002) 8456–8466.
- [29] M. Putti, M. Simonet, R. Solberg, G.W.M. Peters, Electrospinning poly( $\epsilon$ -caprolactone) under controlled environmental conditions: influence on fibre morphology and orientation, *Polymer* 63 (2015) 189–195.
- [30] J. Reignier, M.A. Huneault, Preparation of interconnected poly( $\epsilon$ -caprolactone) porous scaffolds by a combination of polymer and salt particulate leaching, *Polymer* 47 (2006) 4703–4717.
- [31] E.L. Cussler, *Diffusion Mass Transfer in Fluid Systems*, Cambridge University Press, New York, 1997.
- [32] F. Nacimiento, R. Alcantara, G.R. Gonzalez, J.F. Tirado, Electrodeposited polyacrylonitrile and cobalt-tin composite thin film on titanium substrate, *J. Electrochem. Soc.* 159 (2012) 1028–1033.
- [33] S. Lee, J. Kim, B.C. Ku, J. Kim, H.I. Joh, Structural evolution of polyacrylonitrile fibres in stabilisation and carbonisation, *Adv. Chem. Eng. Sci.* 2 (2012) 275–282.
- [34] S.R. Dods, O. Hardick, B. Stevens, D.G. Bracewell, Fabricating electrospun cellulose nanofiber adsorbents for ion-exchange chromatography, *J. Chromatogr. A* 1376 (2015) 74–83.
- [35] L. Deng, R.J. Young, I.A. Kinloch, Y. Zhu, S.J. Eichhorn, Carbon nanofibres produced from electrospun cellulose nanofibres, *Carbon* 58 (2013) 66–75.
- [36] M. Gopiranam, K. Fujimori, K. Zeeshan, B.S. Kim, I.S. Kim, Structural and mechanical properties of cellulose acetate/graphene hybrid nanofibers: spectroscopic investigations, *Express Polym Lett* 7 (2013) 554–563.
- [37] Y. Qiu, K. Park, Environmental-sensitive hydrogels for drug delivery, *Adv. Drug Deliver. Rev.* 53 (2001) 321–339.